

Beamtest of Non-irradiated and Irradiated ATLAS SCT Microstrip Modules at KEK

Y. Unno¹, T. Matuo², T. Hashizaki², T. Akimoto⁸, J. Bernabeu¹⁰, Z. Dolezal⁴, L. Eklund⁹, K. Hara⁸, Y. Ikegami¹, Y. Iwata⁵, Y. Kato⁸, C. Ketterer³, H. Kobayashi⁸, T. Kohriki¹, T. Kondo¹, T. Koshino², J. Ludwig³, T. Masuda⁵, G. Moorhead⁷, I. Nakano², K. Norimatsu², T. Ohsugi⁵, K. Runge³, S. Shinma⁸, R. Takashima⁶, R. Tanaka², N. Tanimoto², S. Terada¹, N. Ujiie¹, M. Vos¹⁰, K. Yamanaka⁵, and T. Yamashita²

¹Institute of Particle and Nuclear Studies, High Energy Accelerator Research Organization (KEK), Tsukuba 305-0801, Japan

²Physics department, Okayama University, Okayama 700-8530, Japan

³Department of Physics, Albert-Ludwig University of Freiburg, D-79104 Freiburg, Germany

⁴Institute of Particle and Nuclear Physics, Charles University, CZ-180 00 Prague 8, Czech Republic

⁵Physics department, Hiroshima University, Higashi-Hiroshima 739-8526, Japan

⁶Education department, Kyoto University of Education, Kyoto 612-0863, Japan

⁷School of Physics, University of Melbourne, Parkville, Victoria 3052, Australia

⁸Institute of Physics, University of Tsukuba, Tsukuba 305-8571, Japan

⁹Department of Radiation Science, Uppsala University, S-75121 Uppsala, Sweden

¹⁰Instituto de Fisica Corpuscular, U. Valencia/CSIC, E-46071, Valencia, Spain

Abstract

Non-irradiated and irradiated ATLAS SCT barrel and endcap modules have been beamtested with 4 GeV/c pions. Pulse shapes confirmed the peaking time of the amplifier to be 22 ns with slight deterioration in the irradiated modules. Median charges saturated around 3.8 fC both in the non-irradiated and irradiated modules. Signal/Noise ratios, using the noise estimates from the in-situ calibration, were >16 in the non-irradiated (>150 V), and >10 in the irradiated (>300 V) barrel modules. No excess common-mode noise was observed.

I. INTRODUCTION

In order to investigate the origin of the mass of elementary particles and search for new physics, a new accelerator, LHC (Large Hadron Collider), is being built at CERN which will accelerate and collide protons at the centre of mass energy of 14 TeV, with a collision luminosity of 10^{34} cm⁻²sec⁻¹ and a beam crossing interval of 25 ns. Two major experiments, ATLAS and CMS, are under construction for the LHC, both aiming to detect all possible charged and neutral particles emerging from the fundamental interactions.

In the ATLAS experiment, the detection and the measurement of momentum of charged particles will be made in the inner detector, consisting of pixel (PIXEL), silicon microstrip (SCT) [1], and transition-radiation (TRT) detectors, inside a 2 Tesla solenoid magnet of a diameter of 2 m at the centre of the ATLAS detector. The SCT provides high-precision tracking information with a position resolution of 23 μ m per sensing plane. It comprises a central barrel section of 4 cylinders and two endcap sections of 9 disks each. The cylinders or disks have two

sensing planes per layer, with total areas of silicon of 34 and 27 m² in the barrel and the endcap sections, respectively. The silicon microstrip sensors will receive a cumulative fluence of 2×10^{14} 1 MeV-neutron-equivalent particles/cm² over 10 years of operation at the inner-most radius of 30 cm from the collision axis.

The silicon planes are implemented in detector units called “modules” made of silicon microstrip sensors and fast-shaping, discriminating readout electronics, combined with electrical, mechanical, and thermal structures. After intensive development following the Technical Design Report [2], a number of realistic SCT modules, fully equipped with SCT-specified components, have become available, of which a significant number have been irradiated to the full fluence of particles.

Two beamtests [3] were carried out at KEK using pion beams of 4 GeV/c at the 12 GeV proton synchrotron, measuring the performance of the fully equipped SCT modules. These were the first beamtests of the SCT modules, prior beamtests having been at the component level [4]. Since the results of the second beamtest supersede and expand on the first, only those of the second test are presented in this paper.

II. SCT SILICON MICROSTRIP MODULES

A. ATLAS SCT silicon microstrip sensor

After intensive studies of the radiation damage in semiconductors and following the development of radiation-tolerant designs, ATLAS SCT has chosen a type of silicon microstrip sensors with p-implant strips in n-bulk silicon wafers, so-called p-in-n sensors. Several geometries of otherwise similar detector technology have been implemented; one, essentially square, is used for the barrel modules, and five different wedge shapes used for the endcap modules. The sensors are designed to have a mean strip pitch of 80 μ m at the centre of a module. The parameters of the barrel and the endcap sensors used in the beamtest are summarized in Table 1 [5].

Manuscript draft Nov. 14, 2001. This work was supported in part by the Grant-in-aid for Scientific Research of Japan Ministry of Education, Science, and Technology, Australian Research Council and Department of Industry, Science and Resources, German Ministry for Education and Research (BMBF), and Valencia University and the Spanish research council CSIC.

Table 1
Parameters of the ATLAS SCT p-in-n silicon microstrip sensors

Module	Barrel	endcap
Sensor type	p-in-n, AC-coupled, Single-sided	
Thickness	285 ± 15 μm	
Shape	square	wedge
Size (outer) (width×length)	63.6mm×64.0mm	71.8/64.7mm×57.5mm 64.6/56.5mm×65.5mm
Bulk	n-type, high resistivity (about 4 kΩcm)	
Strip type	p ⁺	
Strip pitch	80 μm	85.95, 77.45 μm
Strip length	62 mm	55.5, 63.5 mm
Strip width	22 μm	
Number of strips	768 readout + 2 shaping	
Strip AC coupling	SiO ₂ + SiN, >20 pF/cm	
Backside	Uniformly doped n ⁺ layer	

B. Frontend readout ASIC

The signals from the strips are read out by frontend circuits with high gain (50mV/fC), unipolar fast shaping (20 ns peaking time), on-chip discrimination (binary readout), a digital pipeline for the trigger decision delay of 3.3 μs duration, and an eight-event deep derandomising buffer to permit sustained operation at trigger rates up to 10⁵ per second without deadtime. The custom SCT design, the ABCD, is implemented as a BiCMOS single chip application-specific-integrated-circuit (ASIC) in a radiation-tolerant technology [6]. Each ASIC has 128 channels with a common threshold for discrimination.

Following testing of the first generation ABCD, the second generation, ABCD2T, implemented a 4 bit DAC adjustment to the threshold at each channel to reduce excess threshold spread (trim DAC), and shielding the input pads for excess noise protection [7]. The third generation, ABCD3T, fixed poor matching in the circuit which generated the correction voltage for the discriminator threshold, and added a 2-bit range for the step of the trimDAC to cope with the deterioration in the trimming off-set spread after irradiation [8].

C. Barrel and endcap modules

The SCT modules are made from four silicon sensors, glued in pairs on each side of a baseboard for total strip lengths of 12 cm. The two over-lapping planes are slightly rotated with respect to each other by an angle of 40 mrad such that a single space-point is provided for each track at appropriate spatial resolutions while retaining nearly parallel strips. Each module is equipped with 12 ABCD chips on a hybrid, 6 on the top and 6 on the bottom side. In the barrel modules, the hybrid is placed near the centre of the module in a wrap-around configuration; in the endcap modules, the hybrid is placed at one end of the module and is double-sided. The different designs were driven principally by the difference in cylindrical and disk geometries. Photographs of the barrel and endcap modules are shown in Figure 1 and Figure 2.

Thermal management is critical to extract the heat of the

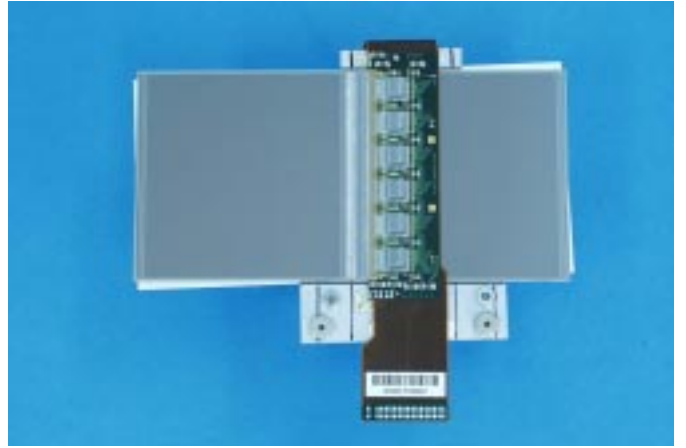


Figure 1: ATLAS SCT barrel module

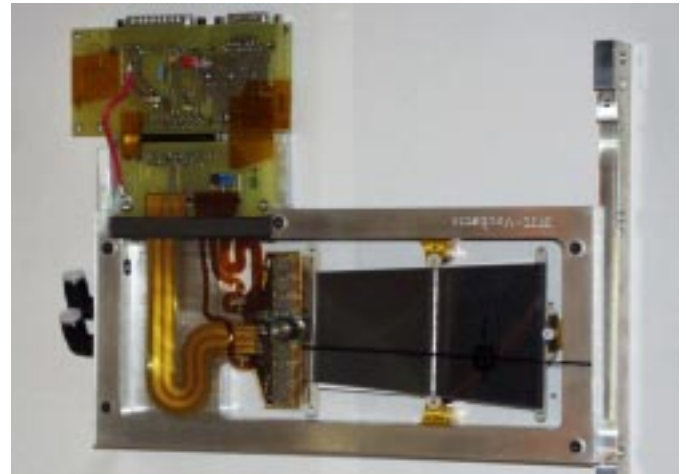


Figure 2: ATLAS SCT endcap module, together with a module frame and a readout card at the beamtest

ASICs (5 to 8 W) and of the sensors, especially after the sensors are heavily radiation-damaged (1 to 2 W). The baseboard with a high thermal conductivity is a key element to prevent the thermal runaway of the sensors. The barrel module is cooled at one area at the wide tab, whereas the endcap module has two small cooling areas: one at the junction of the sensor and the hybrid, and the other at the far-end of the sensors.

Two modules, one barrel and one endcap, were irradiated prior to the beamtest to the fluence of 3×10^{14} protons/cm² at the 24 GeV proton synchrotron at CERN, equivalent to the 2×10^{14} 1 MeV neutrons/cm². The modules were annealed for 7 days at 28 °C to simulate the effects of the warm-up for the maintenance in the real experiment, and apart from several days at room temperature during preparation were otherwise kept cold (<-10 °C).

III. BEAMTEST

A. Setup

Two beamtests were carried out. Two barrel and one endcap modules with ABCD2T chips were tested in the first, and three barrel and three endcap modules with ABCD3T chips, including two irradiated modules, were tested in the second beamtest. The modules are summarized in Table 2 [9].

Table 2

Name, type, ASIC, and irradiation characteristics of the modules in two beamtests

Beamtest	Name	Type	ASIC	Irradiation	
1	k3103	barrel	ABCD2T	non-irrad	
	FR-k81	endcap	ABCD2T	non-irrad	
	k3104	barrel	ABCD2T	non-irrad	
2	mod1	011	ABCD3T	non-irrad	
	mod2	022	ABCD3T	non-irrad	
	mod3	003	ABCD3T	irrad	
	mod4	VAL-k3-166	endcap	ABCD3T	irrad
	mod5	VAL-k3-165	endcap	ABCD3T	non-irrad
	mod6	CG-k3-170	endcap	ABCD3T	non-irrad

The modules were attached to aluminium module frames and positioned in a thermo-box in the beamline. Three analogue readout “Si-telescopes” provide independent tracking with a position resolution of about 5 μm in horizontal and in vertical directions. Pairs of modules, mod2 and mod3, and mod4 and mod5, were sandwiched between telescope planes. The modules or telescopes were spaced at 30 mm intervals. The smearing by multiple scattering was estimated to be negligible by interpolating the positions of the incident particles with two adjacent telescopes. Readout was triggered by scintillators of 2 cm x 2 cm placed upstream.

The modules were cooled in two ways: the overall environment inside the thermo-box was cooled with a circulation of cold air of about -20 $^{\circ}\text{C}$, and, in addition, the irradiated modules were cooled with a liquid cooling of about -13 $^{\circ}\text{C}$. The temperatures of the barrel hybrid were about 0 $^{\circ}\text{C}$.

The temperatures of the sensors were estimated to be about -10 $^{\circ}\text{C}$. Typical leakage currents of the non-irradiated and the irradiated modules were 0.2 μA and 2 mA, respectively. Problems were encountered in cooling the endcap modules, with their hybrids running at about 37 $^{\circ}\text{C}$ and 54 $^{\circ}\text{C}$ in the non-irradiated and the irradiated modules, respectively.

B. Trim range setting in the irradiated modules

After the irradiation, ABCD3T chips showed a problem in setting the trim DAC range of the trim circuitry. (This problem was fixed in the more recent ABCD3TA chips.) The ranges

were stuck to 1 and 2 in mod3, and 2 and 3 in mod4, in the 4 chips illuminated by the beam. The number of channels masked due to this out-of-trimming was, however, small: 1 and 4 channels in the mod3 and the mod4 modules, respectively.

C. Charge calibration

The relations of the threshold voltages and the charges were calibrated, in situ, by injecting charges with the internal circuitry in the ABCD chips. The resulting calibration curves, averaged over the chips in the beam spot, are shown in Figure 3.

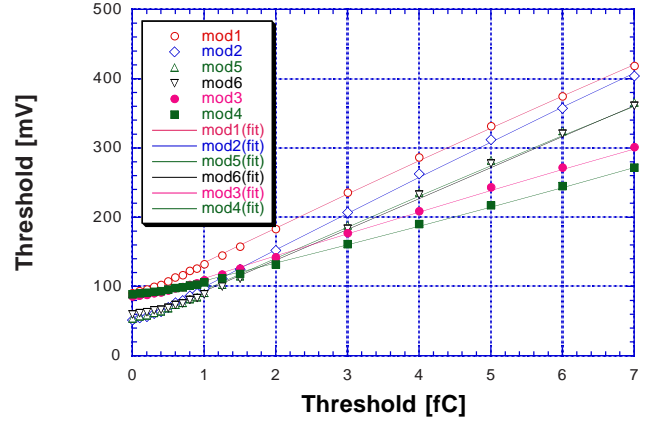


Figure 3: Calibrations of the threshold in mV and fC

The internal calibration circuitry required several corrections: deviation of the capacitance values of the charge injection capacitors, and deviation of charge scales due to the chip temperatures and radiation damage. These factors were measured and/or estimated as in Table 3. The charge scales were multiplied by the “Total” factors.

Table 3

Charge correction factors due to calibration capacitance (Cap), temperature (Temp), irradiation(Irrad), and combined total(Total)

mod	Name	Cap	Temp	Irrad	Total
1	011	1.07	1	1	1.07
2	022	1.07	1	1	1.07
3	003	1.07	1	0.97	1.04
4	166	1.07	0.95	0.97	0.99
5	165	1.07	0.97	1	1.04
6	170	1.07	0.97	1	1.04

D. Data taking and analysis

Two parameters were varied during data-taking: the sensor bias voltage, between 25 and 275 V for the non-irradiated and 150 and 500 V for the irradiated modules, and the threshold between 0.7 and 6 fC. In the following analyses, the conditions

taken for a typical setting were, otherwise mentioned, (1) bias voltages of 150 V and 350 V for the non-irradiated and the irradiated modules, and (2) threshold at 1 fC. In the plots, the voltages of the irradiated modules were corrected for the voltage drops in the series resistance in the bias supply lines.

IV. DATA ANALYSIS

A. Pulse shape reconstruction

The ABCD chip has, after amplification and shaping, discriminator circuitry. The output is sampled at a fixed phase of the 40 MHz clock. Unlike at the LHC where the clock will be synchronised with collision frequency, in the beamtest the arrival time of the triggering particle is random relative to the clock phase. This interval was measured using a TDC which, when combined with the threshold scans, allowed the time distribution of the median pulse heights to be reconstructed.

The resulting time distributions of the median pulse heights are shown in Figure 4 for the non-irradiated (average of mod1 and mod2) and for the irradiated (mod3) modules. In this figure, the offsets of the peaking were adjusted to be at 40 ns. The impulse response curves of a first-order differential and third-order integration circuitry, CR-RC³, were fitted to the rising part of the pulses between 20 and 45 ns. The peaking time of the non-irradiated module was thus found to be 22 ns and that of the irradiated 27 ns. The peaking time of the non-irradiated chips is consistent with the ABCD specification. The peaking time of the irradiated module was longer due to a slower charge collection in the radiation-damaged sensors and a slower speed of the damaged amplifiers.

Another distinctive feature of the reconstructed pulses was the shoulders seen after the peaking. This shoulder could not be reproduced in the simulation of the charge collection in the damaged sensors. Since this shoulder has not been observed in similar chips without the discriminators [10], we surmise it could be a physical feedback from the discriminator. Larger excess shoulders were observed in the endcap modules than in the barrel modules.

The peaking times of the modules as a function of bias voltages were shown in Figure 5. In the non-irradiated modules, the pulses slowed down slightly, by 3 ns, below 150 V to 50 V. The endcap modules were slower than the barrel modules, by 5 ns in the non-irradiated and 7 ns in the irradiated modules. This deterioration might be caused by the higher temperature of the chips in the endcap hybrids.

In the following analyses, events have been selected in which time was in the peak region between 35 and 45 ns. No correction was made to the range in other bias voltages since the move of the peak position was small.

B. Position resolutions

Consecutive hit-strips were clustered within each sensing plane to define a hit-cluster with the geometrical centre as the position of the “cluster centre” and the number of strips as the “cluster width”. The trajectories of the incident particles were

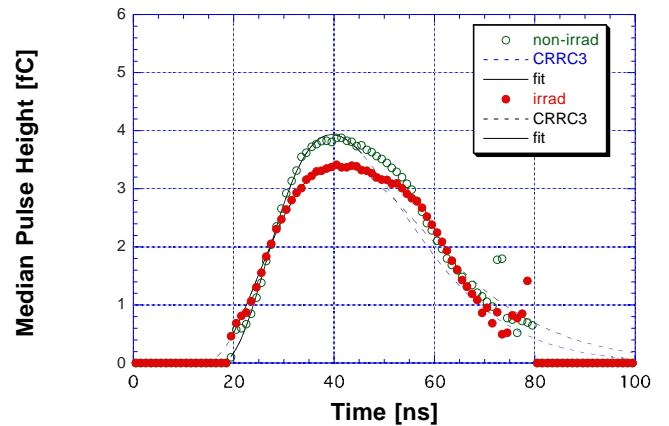


Figure 4: Median pulse height distributions as a function of time between trigger and clock phase: non-irradiated (open circle) and irradiated (filled circle) modules, and the impulse responses of CR-RC³ circuitry (solid line being the fitted region) with the peaking times of 22 and 27 ns, respectively

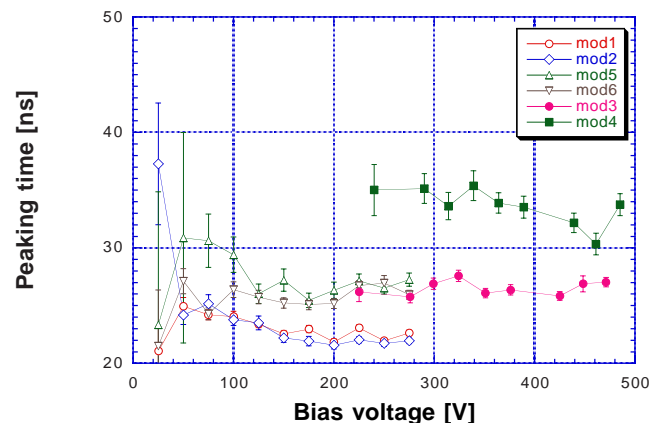


Figure 5: Bias voltage dependence of the peaking times

defined by the two adjacent telescopes in order to minimize the effect of multiple scattering.

The differences of the cluster centres from the projected hit gave the position resolution of the sensing plane. The deviation distributions of one module, mod1, is shown in Figure 6, for all events (circle) and for the cluster width greater than 1, the “multi-hits”, (diamond). The distribution of all events is close to the uniform distribution expected for the pitch of 80 μm . That of the multi-hits is much narrower due to the fact that the predominance of multi-hits from tracks passing midway between the strips, effectively reducing the width of the sensitive region.

In order to derive the root-mean-square (RMS) resolution of the deviations, the Gaussian functions were fitted without weighting, and the Gaussian sigmas were reduced by a factor 1.24 to transform the Gaussian standard deviations to the RMS of the uniform distribution. The resulting RMS resolutions were 22.5 μm and 10 μm for the all and multi-hits events, respective-

ly.

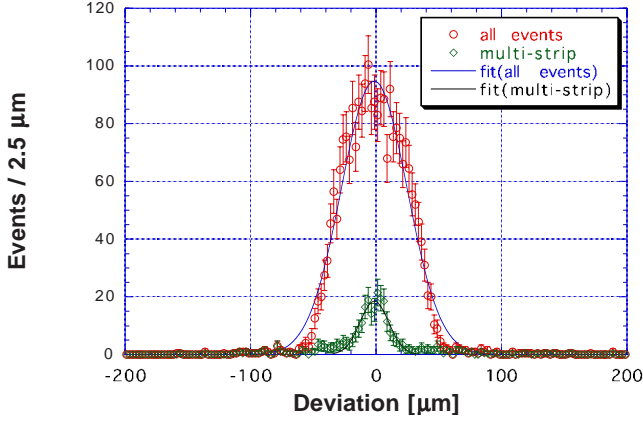


Figure 6: Deviations of the cluster centre from the expected positions of incident particles of the mod1 module: all events (circles) and the events with multi-hits (diamonds), with Gaussian fits without weighting

In analysing the endcap modules, a correction to the fan geometry was taken into account to project the hit at $t=(x, y)$ to the x axis defined at a pitch, p , approximated as

$$xp = x + ((d\theta)/(dx)) \cdot x \cdot y. \quad (1)$$

The pitch evaluated was $86 \mu\text{m}$ at the beam spot.

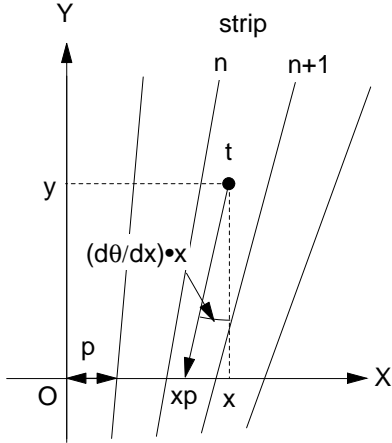


Figure 7: Correction of the fan geometry. A hit at $t=(x, y)$ is projected at the hit x_1 at the x -axis of the pitch p , approximated as $xp=x+(d\theta/dx)\cdot x\cdot y$

The RMS resolutions are shown in Figure 8 and Figure 9 as a function of bias voltage and threshold. Those of the modules outside the telescopes were corrected for the multiple scattering effect. The RMS resolutions of the barrel and the endcap modules were about $23 \mu\text{m}$ and $26 \mu\text{m}$, consistent with their pitch of $80 \mu\text{m}$ and $86 \mu\text{m}$, respectively, although those of the endcap modules were slightly worse than the expected.

There was very little dependence on bias voltage in the non-irradiated modules, while those of irradiated modules showed an improvement at reduced bias voltage. The dependence on the threshold was a bit complicated: the resolutions were better both below and above 1.5 fC . This can be understood as the combined effect of fraction of multi-hits and the loss of efficiency where the former increases events in narrow distributions while the latter reduces the sensitive widths.

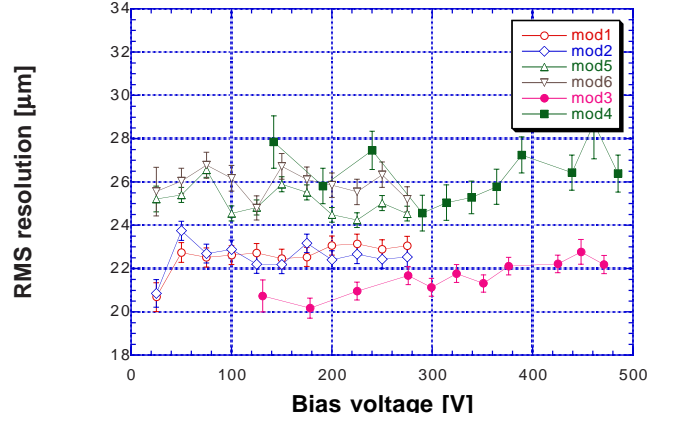


Figure 8: RMS resolutions as a function of bias voltage.

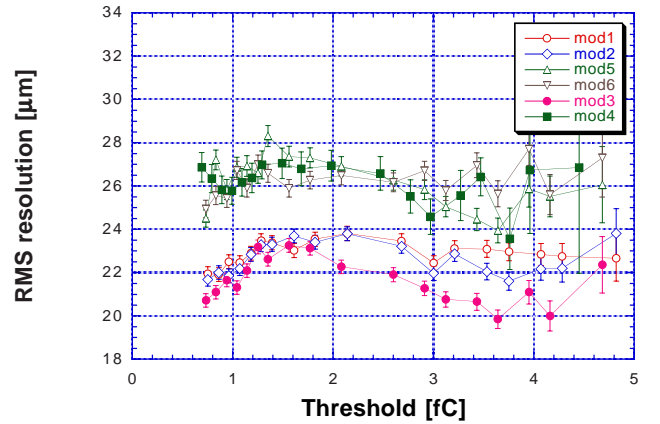


Figure 9: RMS resolutions as a function of threshold.

C. Mean cluster width

The multi-hits events had better resolution due to the effectively narrow sensitive width. The fractions of the multi-hits, parameterized as the mean cluster width, are shown in Figure 10 and in Figure 11 as a function of bias voltage and threshold. The trends seen in the RMS resolutions can be confirmed.

D. Efficiency scans and Median charges

By counting hits with cluster centres within a window of the incident particles (full width of $500 \mu\text{m}$ in the analysis), the efficiency at a threshold can be obtained. The pulse height (Land-

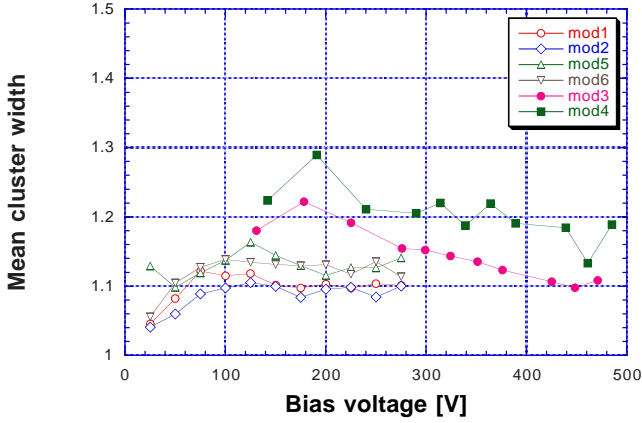


Figure 10: Mean cluster widths as a function of bias voltage

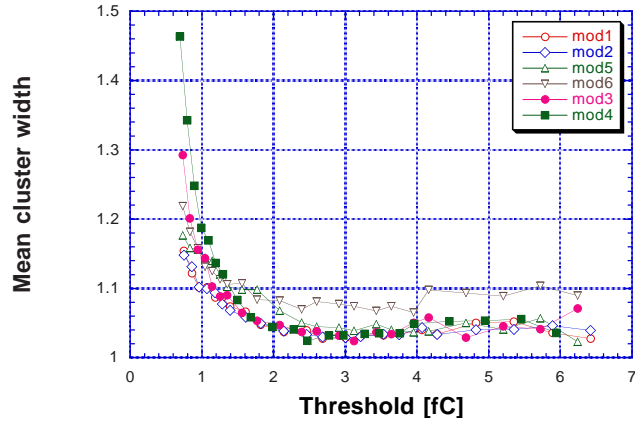


Figure 11: Mean cluster widths as a function of threshold

au) distribution is reconstructed as an efficiency curve by scanning the threshold. An example is shown in Figure 12 for the irradiated module, mod3, where with the bias voltage is also scanned. The threshold of the 50% efficiency is the median charge of the pulse height (Landau) distribution.

In order to obtain the threshold of 50% efficiency, a modified error function, eq. (2), was fitted to the efficiency scans,

$$eff(q) = p_3(1 - erf(T \cdot f(T))) \quad (2)$$

where

$$f(T) = 1 + 0.6 \cdot \tanh(-p_4 \cdot T) \quad \text{and} \quad (3)$$

$$T = (q - p_1) / (\sqrt{2} \cdot p_2). \quad (4)$$

The function, erf , was the integral of the Gaussian distribution. The function, $f(T)$, is an empirical function to modify the Gaussian to the Gaussian-convoluted Landau distribution. The fitting parameters expressed the median (p_1), the width (p_2), the saturation (p_3), and the skew (p_4).

The median charges of the modules obtained are shown in Figure 13 as a function of the bias voltage. The median charges of the non-irradiated modules saturate above 150V to the charg-

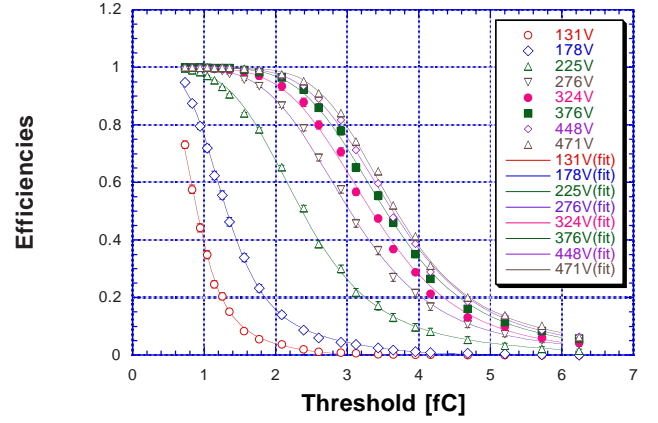


Figure 12: Threshold scan of the efficiencies at various bias voltages in the irradiated barrel module, mod3. The lines are fits to the empirical formula in the text

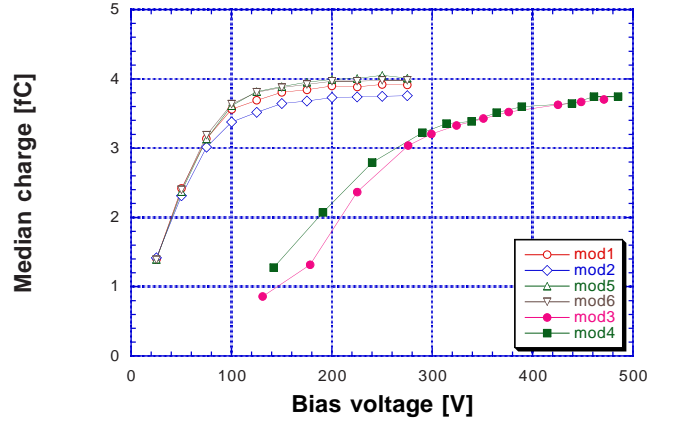


Figure 13: Bias voltage dependence of the median charges.

es between 3.8 fC and 4.0 fC. The saturations of the median charges of the irradiated modules were slower, reaching around 3.8 fC at 500V. The full depletion voltages of the non-irradiated and irradiated sensors were about 70 V and 300 V, respectively.

The median charges of the two non-irradiated barrel modules do not coincide, nor do those of the barrel and the endcap modules. These differences could be attributed to the chip-by-chip variation of the calibration capacitance and insufficient corrections on calibration scales due to temperature and radiation damage.

E. Noise occupancies and ENC

Hits which were out of time (time < 15 ns) and out of track window ($2 \cdot \text{efficiency window}$) were counted as noise hits due to electronics noise. The resulting number of hit strips was divided by the number of strips outside the track window to obtain the noise occupancy. The noise occupancies of the modules are shown in Figure 14 as a function of threshold-squared. The noise occupancies at 1 fC of the non-irradiated modules were

below 1×10^{-4} and that of the irradiated barrel module was below 1×10^{-3} . Those of the endcap modules were an order larger than of the barrel modules which could be attributed to the difference in chip temperatures.

The relation between the noise occupancy and the threshold-squared is a straight line in logarithmic scale of occupancy because the occupancy can be approximated as

$$\text{occupancy}(q) \propto \exp(-(1/2)(q/\sigma)^2) \quad (5)$$

where σ is the equivalent-noise-charge (ENC) of the amplifiers.

The resulting ENCs of the modules had little bias voltage dependence. The averaged ENCs above 100 V (non-irrad) and 300 V (irrad), occuENC, are summarized in Table 4. The ENCs were obtained separately in the in-situ calibration, calibENC, with an average of ENCs at 1, 2, and 3 fC, including the corrections in the section III.C. In comparison, calibENCs were systematically larger than occuENCs, which is yet to be understood.

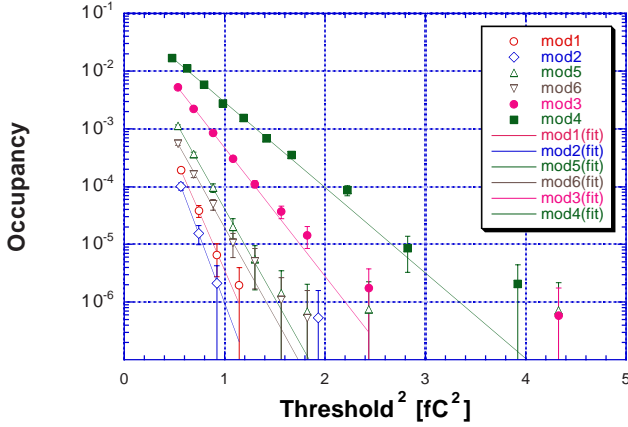


Figure 14: Noise occupancies as a function of $(\text{threshold})^2$. The lines are fits to the function, $\exp(-1/2*(th/\sigma)^2)$

Table 4

Comparison of ENCs obtained from the occupancy and the in-situ calibration

mod	occuENC[fC]	calibENC[fC]	Ratio
1	0.239	0.245	0.976
2	0.222	0.234	0.949
3	0.311	0.342	0.910
4	0.385	0.411	0.937
5	0.264	0.291	0.907
6	0.264	0.290	0.910

F. Signal-to-Noise ratios

One way of cancelling the uncertainty of the calibration capacitance is to take the ratio of the median charges to the ENCs,

the signal-to-noise ratios (S/N). The S/N ratio is also an indicator of the performance since a $S/N > 9$ is required in practical use from experience. In order to calculate the S/N, the worse ENCs, calibENC, were used to be conservative. The resulting S/N ratios are shown in Figure 15 as a function of bias voltage.

A good match of the S/N was seen between two barrel and two endcap modules, which supported the differences of the median charges were caused by the chip-to-chip variation of the calibration capacitance. The $S/N > 16$ was reached above 150 V in the non-irradiated barrel, and the $S/N > 10$ above 300 V in the irradiated barrel modules. The S/N of endcap modules were considerably lower than those of barrel modules, which can be attributed to the higher chip temperatures.

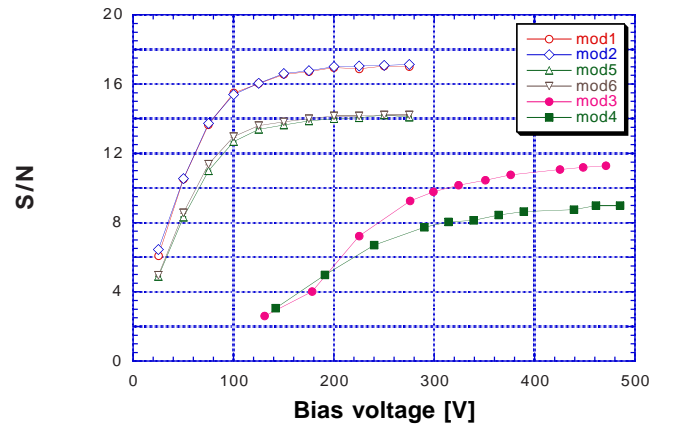


Figure 15: Signal-to-noise ratios as a function of bias voltage. The noises were averages of 1, 2, and 3 fC of the in-situ calibration

G. Charge collection in the interstrip regions

Since the charges moving in the region between two strips generate currents in both strips, the charges induced are halved, and thus the efficiency is reduced. This is seen in Figure 16 where “eta” is the normalized distance from the strip centres. Degradations were seen in high thresholds, however, the efficiencies were still high at 1 fC, the expected operating threshold. The ratios of the median charges in the strip and the interstrip region were about 0.95 and 0.85 in the non-irradiated and the irradiated modules. The thresholds where the loss of efficiency starts could be estimated by applying these factors to the efficiency curves, e.g., in Figure 12.

H. Common-mode noises

If the electronics system has an external noise pick-up or an internal oscillation, noise appears as a multiple hits across many strips, a common-mode noise. The distributions of number of hits in the non-irradiated (average of mod1 and mod2) and irradiated (mod3) modules are shown in Figure 17 at the threshold of 0.7 fC. No excess tail of a common-mode noise was observed.

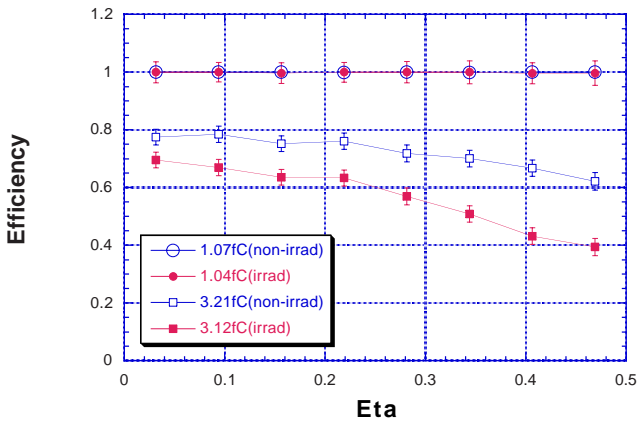


Figure 16: Efficiencies between the strips. “Eta” defines the distance from the strips: 0 at strip and 0.5 at midway.

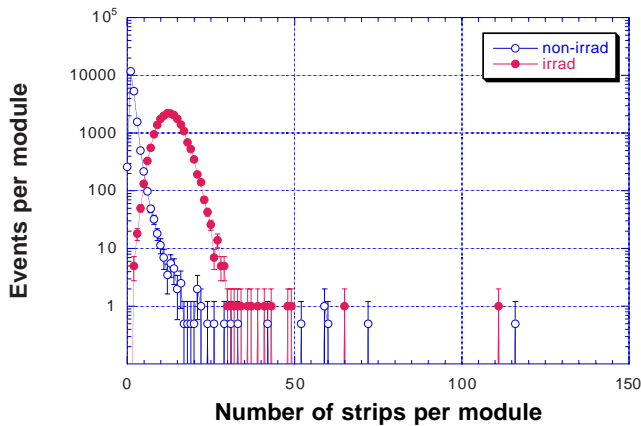


Figure 17: Distribution of the number of strips hit in the non-irradiated (average of mod1 and mod2) and irradiated (mod3) modules at 0.7 fC thresholds

V. SUMMARY

Two beamtests were carried out by using 4 GeV/c pions from the 12 GeV proton synchrotron at KEK for the ATLAS SCT barrel and endcap modules fully equipped with the SCT specification components, including modules irradiated to a fluence of 3×10^{14} protons/cm², the equivalent fluence expected in the operation of 10 years in the ATLAS detector at LHC.

A pulse shape analysis confirmed the peaking time of the amplifier to be 22 ns in the non-irradiated modules with deteriorated to 27 ns in the irradiated modules. An excess shoulder in the pulse shapes was observed which could be feedback from the discriminator. The RMS position resolutions were consistent with the uniform distribution at the pitch of 80 μ m in the barrel and of 86 μ m in the endcap at the beam spot. The variations of the resolutions were correlated to the fraction of the multi-hits events in the interstrip region where much better resolutions is expected.

The median charges of the pulse height (Landau) distribution

were obtained from discriminator threshold scans, and saturated around 3.8 fC in the non-irradiated (>150 V) and irradiated (500 V) modules. The noise occupancies at 1 fC were below 1×10^{-4} in the non-irradiated and below 1×10^{-3} in the irradiated barrel modules. The ENC_s obtained from the noise occupancies were systematically lower than those obtained from the in-situ calibration, an observation requiring further investigation. Using the median charges and the ENC_s of in-situ calibration, the signal-to-noise ratios were >16 in the non-irradiated (>150 V) and >10 in the irradiated (>300 V) barrel modules. The matching of the S/N of the non-irradiated modules indicated the spread of the median charges were caused by the variation of the chip-by-chip calibration capacitance.

The endcap modules were worse in two respects: (1) rise times of the pulses and larger excess shoulders, and (2) ENC_s. These are attributed to much higher temperatures of the readout ASICs.

No excess common-mode was observed in the beamtests.

VI. ACKNOWLEDGEMENT

The authors wish to acknowledge the cooperation of the beam channel crews of the d π 2 beamline of the KEK PS and support from the ATLAS SCT collaboration.

VII. REFERENCES

- [1] Y. Unno, “ATLAS silicon microstrip Semiconductor Tracker (SCT), Nucl. Instr. Metho. A453, pp.109-120, 2000
- [2] ATLAS Inner Detector Technical Design Report, CERN/LHCC/97-17, ATLAS TDR 5, 30 April 1997
- [3] Y. Unno et al., (1) Testbeam experiment T450, KEK, 10-20 Dec. 1999, (2) Testbeam experiment T478, KEK, 28 Nov.-10 Dec. 2000
- [4] Y. Unno et al., “Evaluation of Radiation Damaged P-in-n and N-in-n Silicon Microstrip Detectors”, IEEE Trans. Nucl. Scie., Vol. 46, pp. 1957-1963, 1999
- [5] Sensors fabricated by Hamamatsu Photonics, 1126-1, Ichino-cho, Hamamatsu-shi 435, Japan
- [6] DMILL technology, TEMIC Semiconductors, La Chantre-rie, F-44306 Nantes, France
- [7] F. Anghinolfi et al., “Performance of the Electrical Module Prototypes for the ATLAS Silicon Tracker”, Snowmass 1999, Electronics for LHC experiments, pp. 118-122
- [8] W. Dabrowski et al., “Design and Performance of the ABCD Chip for the Binary Readout of Silicon Strip Detectors in the ATLAS Semiconductor Tracker”, IEEE Trans.Nucl.Sci. Vol. 47, pp. 1843-1850, 2000
- [9] The FR-, VAL-, and CG-modules were prepared by Univ. Freiburg, Univ. Valencia, and CERN-Univ. Geneva, respectively. The rest of the modules were by KEK
- [10] W. Dabrowski, private communication